Observations of plasma dynamics in the vacuum spark

H. Chuaqui, M. Favre, E. S. Wyndham, R. Aliaga Rossel, Ian Mitchell, and L. Soto

Citation: Physics of Plasmas **2**, 3910 (1995); doi: 10.1063/1.871020
View online: https://doi.org/10.1063/1.871020
View Table of Contents: http://aip.scitation.org/toc/php/2/10
Published by the American Institute of Physics

Observations of plasma dynamics in the vacuum spark

H. Chuaqui, M. Favre, and E. S. Wyndham
Facultad de Física, Casilla 306, Pontificia Universidad Católica de Chile, Santiago 22, Chile

R. Aliaga Rossel and Ian Mitchell
The Blackett Laboratory, Imperial College, London SW7 2BZ, United Kingdom

L. Soto
CEN La Reina, Comisión Chilena de Energía Nuclear, Casilla 188-D, Santiago, Chile

(Received 3 April 1995; accepted 20 June 1995)

Experimental observations are presented of a vacuum spark driven by a low impedance pulse forming line delivering 100 kA to the load. A pulsed laser is used to form a preionizing plasma on the cathode. The combination of axial and radial optical streak camera observations, together with the time and space resolved soft x-ray emission, permit the evolution of the plasma dynamics, density and temperature to be measured. Three kinds of behavior are observed according to axial position. A close correlation is found between the x-ray and the optical emission, with the observation of micropinch formation. A discussion is presented in which the behavior of the vacuum spark under differing operating conditions is compared.

I. INTRODUCTION

The very dense hot metallic plasmas observed to form on the nanosecond time scale have made the vacuum spark attractive, both to the experimental physicist as well as to the theoretical physicist. In particular, the observation of radiative collapse with terminal densities of up to 10^{23} cm^{-3} and the temperatures in the keV range have stimulated various theoretical treatments. Both theoretical and experimental work have been reviewed in considerable detail.[1,2]

While the majority of vacuum spark discharges have used low inductance capacitor banks, with a quarter-period time of approximately 1 μs, some research has been performed using a switched water coaxial pulse forming line, with discharge currents of order 100 kA with a pulse length between 50 (Ref. 3) and 140 ns.[4] More recently, the vacuum spark has been operated in the hybrid mode in which the vacuum spark is driven by a water coaxial line, but without a line gap.[5] In this case, the fast transition to conduction of the discharge itself switches the line. Experimental observations have been reported, in particular, of measurements of the electron density and of the x-ray emission under these conditions. These measurements have allowed some understanding of the different plasmas that develop both before, during, and after the emission of x rays from micropinches that coalesce in a Z-pinch column in the part of the discharge that is formed from the midpoint between the electrodes to the cathode.

In the present work we present observations of the plasma dynamics, as obtained using an optical streak camera, together with observations of the x-ray emission. The use of both axial and radial streak photographs provides a better picture of the plasma motion. The x-ray emission from different regions may also be compared with previously published interferometric measurements, as will be detailed in the following sections. The advantages of using a streak camera are in the ability to follow the temporal and spatial evolution of the plasma optical emission in a continuous way. The very short duration pulse associated with emission from a micropinch is easily detected, whereas a single or even multiple frame interferogram will usually not coincide with such an event. A number of new findings with respect to the dynamics of the formation of the Z-pinch column are reported. These include, first, differences in the radial compression velocity as a function of the axial position; second, the observation of the axial propagation of the micropinch formation; and third, the close temporal correspondence between the x-ray emission and the formation of bright emission regions in the Z-pinch column.

II. EXPERIMENTAL DETAILS

The results presented here were all obtained in the hybrid mode of operation.[5] The experimental arrangement is similar to that described in Ref. 5. The initial preionizing plasma conditions were established using a Nd:YAG laser pulse of 0.5 J, incident on the front surface of the cathode. The laser is focused through a 2.5 mm diam hole in the conical anode onto the surface of the cathode. It has been found, since the work published in Ref. 5, that the best operating conditions, in terms of dense Z-pinch plasma formation and of the intensity of the micropinches, are obtained with a slightly defocused laser spot with a diameter of 0.15 mm. This condition corresponds to a power of 3.5×10^{11} $\mathrm{W\,cm}^{-2}$. Both electrodes were made from titanium. The use of a slightly defocused spot has the added advantage, in that the surface erosion of the titanium blank, of 2 mm thickness used as the cathode, is substantially reduced. Over 100 discharges may be made before replacement is required, due to the perforation of the electrode.

The laser pulse was applied approximately 200 ns after the Marx generator begins to charge the line. This interval corresponds to an applied electrode voltage of between 80 and 100 kV. If the laser pulse is applied earlier, the discharge does not switch the line effectively and the current has a lower rate of rise. If the laser pulse is applied later than 300 ns after the start of the charging of the line, there is a greatly enhanced emission of x rays from beam target interaction

 1070-664X/95/2(10)/3910/7/$6.00

without a significant increase in x-ray emission from the plasma volume. The voltage and current traces will be presented below, together with the x-ray emission traces and other diagnostics. It should be noted that the voltage is not measured at the anode, but at a point in the line so that it gives only an approximation to the anode–cathode voltage. An electrode separation of 7 mm was used for the results presented here. The behavior of the discharge is very similar for separations between 6 and 9 mm. For separations of less than 5 mm, however, a dense pinch is observed, but with a greatly reduced x-ray emission and with no observation of micropinch or hot spot formation. For separations over 1 cm, the pinch density is noticeably lower, the discharge impedance is higher, and the lower current does not permit the conditions necessary for micropinch formation.

The soft x-ray emission was observed by two methods. First, the broadband emission was observed using fast Silicon PIN (P-type intrinsic N-type) diodes. One of these, manufactured by Quantrad, was masked to observe emission from the three millimeters closest to the cathode. The mask, however, was not effective in blocking x rays with a characteristic energy of over 40 keV. In addition, an array of fast, small area PIN diodes were used to monitor the emission from the whole volume. The diodes used were the widely available BPX 65 designed for detection of optical signals with a subnanosecond response, but with their glass windows removed to allow response to x-ray emission.[6] In this work, the broadband emission spectrum corresponding to a filter of 5 μm Al foil is presented, both for the Quantrad large area diode and one of the small area diodes, referred to in the following text as BPX.

A second method was implemented to obtain the spatial resolution of x-ray emission in different energy bands by using a pinhole camera, with four different apertures and filter combinations, as listed in the relevant figure caption. The range of observation of x rays by this method extends to approximately 3 nm. The hard x-ray emission was detected using a piece of Pilot-u scintillator covered with 1.5 mm of Al sheet.

The optical streak camera used in these measurements was manufactured by Kentech Instruments. This camera model has a strong maximum sensitivity to green light, with almost no sensitivity in the near ultraviolet. The lack of sensitivity precluded the observation of x rays using scintillator conversion. One to one imaging of the discharge onto the photocathode was implemented. A slit of 0.3 mm diam was used, and sweep speeds of either 7.5 or 2.8 ns/mm were found to be optimum, allowing a maximum temporal resolution of 0.8 ns. Both axial streaks centered on axis and radial streaks were taken at different axial positions. The images were recorded on film for subsequent scanning. Different degrees of neutral density filter were applied to cover the wide dynamic range in emission intensity. The laser pulse that initiates the discharge, was also used to synchronize the optical streak camera with the oscilloscopes and to provide a time reference mark on the streak photographs.

III. EXPERIMENTAL OBSERVATIONS

The results from an axial streak are presented in Fig. 1.

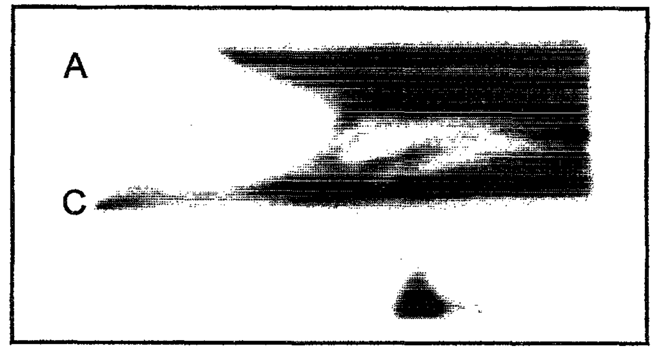

FIG. 1. An axial optical streak camera photograph with a full sweep time of 300 ns. The sweep is from left to right with moderate temporal linearity. A laser-derived fiducial mark indicates a time close to that of maximum current. The anode is indicated as "A" and the cathode as "C."

The first emission is from the laser plasma generated on the surface of the cathode. The first emission from the anode, however, occurs later and is observed approximately 100 ns after the cathode emission, when the discharge current has reached 50 kA. From this moment on, a plasma is seen to expand from both electrodes with similar velocities. A notable increase in the acceleration is observed just before the plasma bridges the whole region for a short time of typically 5–8 ns. When this occurs, the current has a value of 75 kA at a time of approximately 60 ns before the peak current. The value of the apparent axial velocity of the visible plasma prior to the "bridging" event varies from 1 to 8×10^7 cm/s.

At the time of the formation of this "bridging" emission, a further observation may be made: A chain of bright emitting regions are seen to form. These emit in succession, and the position of each individual bright region moves toward the anode, from an initial position of approximately 1.5 mm from the cathode, terminating between 3 and 4 mm from the cathode. The axial velocity of this emission ranges from 3 to 20×10^6 cm/s. Sometimes it is possible to distinguish these regions well, but at other times they blur into each other appreciably. The final blob in this chain occurs within 15 ns after the maximum value of the current.

In addition to the chain of bright emitting regions, a volume of visible plasma, with no visible fine-scale structure, is also seen to propagate from the cathode, starting at the moment of the bridging or connecting plasma. This third region of emission has front velocity of about one-half that of the chain of bright spots. At no time in the discharge does the anode plasma show the same degree of fine structure, as is seen in the half of the discharge closest to the cathode. There is always an appreciable spatial separation between the plasmas originating from both the anode and the cathode, for at least 50 ns after the formation of the connecting or bridging plasma.

The streak camera observations may be associated with the x-ray emission, as shown in Fig. 2. In this figure, both the x-ray and the optical emission, for the same shot as that of Fig. 1, are plotted, together with the voltage and current waveforms. The optical emission shown in Fig. 2 is the sum of the emission between 1.5 and 3.5 mm from the cathode. This procedure emphasizes the more structured part of the

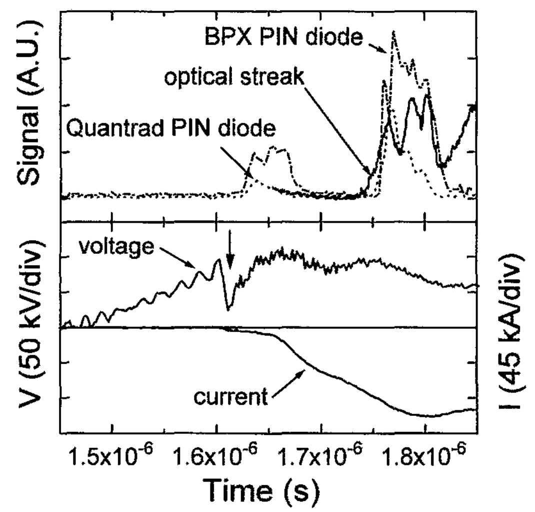

FIG. 2. The x-ray emission from all the vacuum spark (BPX) and from close to the cathode (Quantrad) is compared with the optical emission, as seen in Fig. 1, as well as the current (45 kA/div) and the voltage (50 kV/div). The filter for the x-ray detectors is 5 μm Al. The preionizing laser pulse is shown with an arrow.

optical emission. It is clear from the figure that the emission from the "bridging" plasma occurs almost simultaneously with, to within 10 ns, the start of the x-ray emission, at a time of 1.75 μs. It is also striking that there is a close correspondence between the maxima seen by the PIN diodes and the optical emission. The first maximum in the light emission at this time, coincides with the first maximum in the masked Quantrad signal and with the maximum in the BPX PIN diode. The following maxima, as recorded by the masked Quantrad diode, are successively smaller, while the unmasked (BPX) diode signal remains with a similar amplitude. This is consistent with the hypothesis that the emission of x rays coincides with the optical emission. In this situation, as a result of the detector geometrical arrangement, only the first bright emitting region of the chain will be fully visible to the Quantrad diode, while later regions, successively closer to the anode, will be correspondingly less visible. However, all the emitting region will be equally visible to the unmasked BPX diode, which observes all the discharge volume. The position of the emitting regions is also found to be consistent with the x-ray pinhole photographs, as will be discussed later. The BPX diode signal is seen to have more structure than the Quantrad signal. There are two reasons for this. First, the effective response time of the BPX diode is 1 ns, whereas that of the Quantrad is 3 ns. Second, it is expected that the x-ray pulses observed from the anode and from the anode plasma are generated by two different mechanisms; that of electron beam–target interaction and by Joule heating. In this context, it may be noted that the hard x-ray detector gives a signal at early times when the interelectrode voltage is high; these x rays originate from a comparatively low current of high-energy electrons, giving rise to beam–target x-ray emission. However, the characteristic very hard x-ray pulse with nanosecond duration,[7] associated with micropinch formation in low inductance vacuum spark discharges, is not observed in the vacuum spark configuration of this experiment.

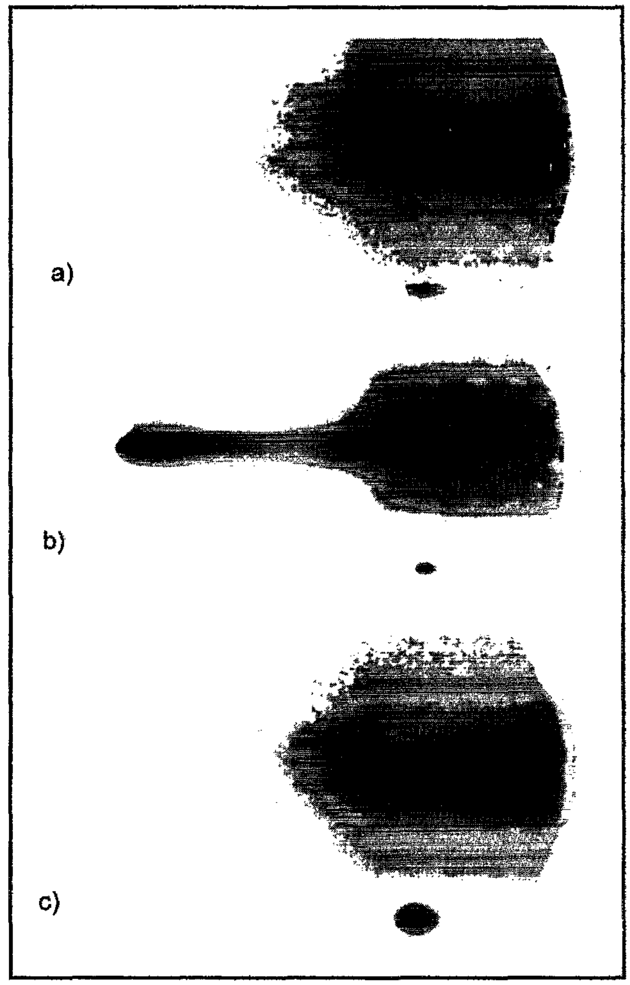

FIG. 3. A series of radial optical streaks at three axial positions: (a) at the midpoint, (b) 1 mm from the cathode, and (c) close to the anode. The full sweep is for 300 ns. The laser fiducial mark indicates a time within 10 ns of the current maximum.

A series of radial streaks are presented in Fig. 3 for three different axial positions: the midpoint; close to the cathode; and third, close to the anode. It will be seen that the different phenomenology for each region, as observed in the case of the axial streaks, is complemented by the axial streak shown in Fig. 1. In Fig. 3(a), an example of a radial streak is shown for the same conditions of operation as above. This streak photograph shows the optical emission at 3.5 mm from the cathode, which is the midpoint of the discharge. The formation of a pinch on axis is clearly visible. The visible shell has an initial diameter of 5 mm. The visible emission from the compressional phase lasts 40 ns and continues for a similar period from the compressed plasma. The external diameter in the pinched down phase is less than 1.5 mm. This value is probably an overestimate, as the visible emission, during the phase when the pinch attains its maximum compression, increases abruptly and saturates the camera. This occurs approximately 30 ns before the maximum of the current. Concurrent with the shell reaching the axis, an off-axis plasma is

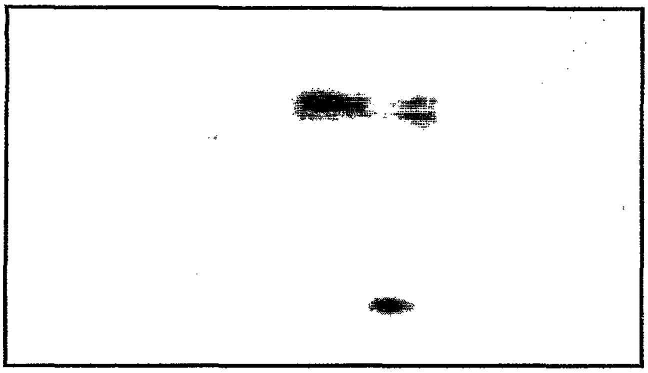

FIG. 4. A radial streak taken 2 mm from the cathode, but with 30 times more light attenuation than used in Fig. 3.

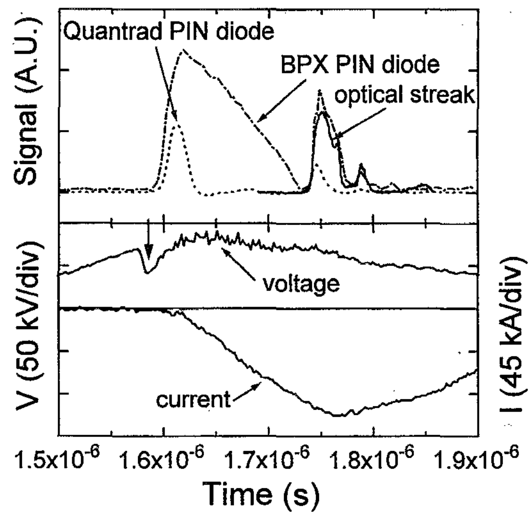

FIG. 5. The x-ray emission from all the discharge (BPX) and from close to the cathode (Quantrad) are compared with the optical emission, taken from Fig. 4. In addition, the current trace (90 kV/div) and the voltage trace is shown. The preionizing laser pulse is shown with an arrow.

seen to form. This has an initial diameter of approximately 3 mm, but expands to about 4 mm in the remaining portion of 150 ns of the sweep. The radial collapse velocity in the pinching phase is 7×10^6 cm/s.

A considerable difference may be seen in behavior on comparing the radial streak for a position close to the cathode; this is shown in Fig. 3(b). Here, we observe an intense emission for 170 ns before the onset of pinching. This coincides with the emission observed in the axial streak for the corresponding position close to the cathode, as seen in Fig. 1. The pinching phase is seen to last for 35–40 ns, but the initial diameter is lower than that of the midpoint, with a value of 3.7 mm. The radial velocity is measured to be 1.2×10^6 cm/s. The sudden increase of light emission is observed, as at the midpoint streak, when the pinch reaches the axis. However, at this position, close to the cathode, there is no evidence of the off-axis plasma seen in the previous case.

The observed emission from the half of the discharge closest to the anode is represented in the streak of Fig. 3(c) taken at a position 3 mm from the anode. The Z-pinch shell is now indistinct and asymmetrical. Emission from the bright pinched region is, however, seen and lasts for 30 ns. As at the former two positions, the emission has the same characteristic increase of light output over the whole width of the exposure. The brightest emission here is found to correspond to the maximum compression. At the position of Fig. 3(c), 3 mm from the anode, the collapsing Z-pinch shell is just visible, whereas, closer to the anode, at a distance of 1.5 mm, it is not. At 3 mm from the anode, the start of the off-axis emission, seen in Fig. 3(a), coincides with maximum pinch compression, whereas closer to the anode the region is both more extensive and appears earlier with respect to the current signal. It is interesting to note that, close to the anode, there is emission on axis, from a 2 mm diam expanding channel, after the time corresponding to the maximum compression at positions closer to the cathode. This could be caused by plasma outflow, or by electron beams, from the pinch column observed to form closer to the cathode.

More understanding of the plasma motion is obtained by taking a series of radial streaks with an increased attenuation of the light input. In Fig. 4 a radial streak taken at a position of 2 mm from the cathode is presented. This is a position where hot spots are preferentially observed. The attenuation in this streak is 30 times the set of radial streaks shown in Fig. 3. The Z-pinch compression phase is no longer visible and the off-axis plasma, when observed, is much less intense than the two groups of bright emission. These appear to be several bright emitting regions run in to each other. The first group of bright spots have a diameter of 0.07 cm, while the second, both less intense and more diffuse, spot has a diameter of 0.14 cm. The light from the first group of bright spots saturate the camera.

The temporal relation between the light emission and the x-ray emission for the shot of Fig. 4 is presented in Fig. 5. On comparing the two wavelengths, we find an almost one to one correspondence between the optical and the x-ray emission. The optical emission is found to have more structure and noticeably faster rise and fall times than the x-ray diode signals; in particular, the fall time is between two and three nanoseconds.

The position of the x-ray emitting plasma may be identified from the pinhole photographs reproduced in Fig. 6. The photographs, using Kodak DEF film, were taken over five consecutive discharges, with a different filter for each of the four images. The beam target emission, which occurs at early times in the discharge from the conical anode, is a clearly visible feature on all the images. An emitting point is seen on the cathode surface, where the laser is focused. The formation of the x-ray emitting Z pinch from one to four millimeters from the cathode is also clear. The micropinch (following the terminology of Ref. 2) closest to the cathode is the brightest feature in all four filters. The streak camera results indicate that this micropinch is the first to form. The diameter of the column, as seen in the image filtered with 10 μm Al foil, taking into consideration the pinhole diameter of 50 μm, is less than 40 μm. The emission from the anode is nearly uniform across the surface, but a more diffuse emitting region is seen in front of the anode in images "a" and "d." The center of this plasma appears to be shifted with respect to the axis. The temperature may be obtained from

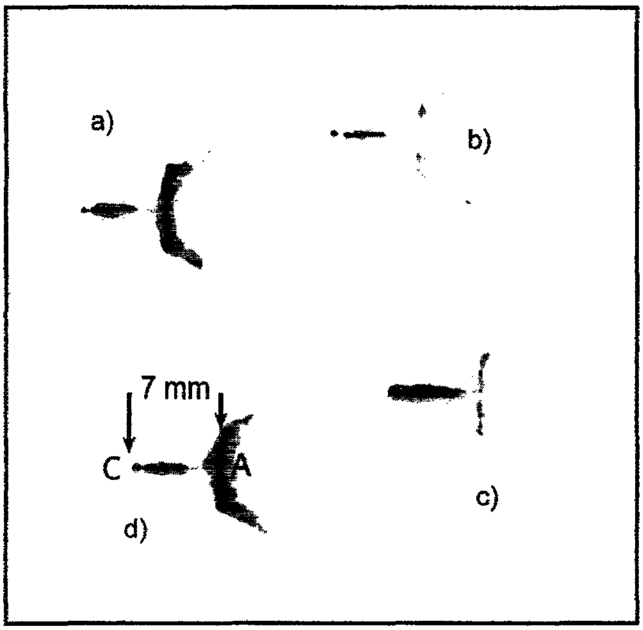

FIG. 6. Four x-ray pinhole images integrated over five consecutive shots. The anode is indicated as "A" and cathode "C." The filters used are (a) 1.5 μm Al and 0.4 μm Zn; (b) 10 μm Al; (c) 2 μm Ti; and (d) 50 μm Be. Images (a) and (b) used a 50 μm diam pinhole, while images (c) and (d) used a 0.1 mm diam pinhole. The camera demagnifies the image by 4.5.

the combination of filters, by either considering the emission to be bremsstrahlung or better, by taking into account the full emission spectrum of free–free, free–bound, and bound–bound transitions.[8] The calculated spectrum may, in turn, be convolved with the filter transmission function and with the film sensitivity in the usual way. Such a code has been developed using a Collisional Radiative Equilibrium, CRE, code, RATION,[9] for an emission spectrum, including the K-shell transitions. The procedure of Ref. 8 offers a considerable refinement in the measurement of the temperature, as well as, in a more limited way, the electron density. This is particularly useful when spectroscopic observation of the x-ray emission is not available. In this work, the RATION suite of codes was used to predict the x-ray spectrum, including the principal line intensities, and folding this with the filter absorption as referred to above. The characteristic temperature in the micropinches is found to be approximately 700 eV, if it is assumed that the electron density is of order $10^{21}-10^{22}$ cm^{-3}. The Z-pinch column is seen to be of appreciably larger diameter in the image filtered with a 2 μm Ti foil. Titanium has a long-wavelength transmission window between 2.3 and 3 nm, which is not the case for the other filters. We may infer, therefore, that this feature is from a colder and possibly longer lasting plasma with a characteristic diameter of approximately 0.8 mm. Time-resolved observation of the x-ray emission from this region will clarify the situation.

IV. DISCUSSION

The results presented here may be compared with earlier observations of the plasma electron density obtained with holographic interferometry[5] for the vacuum spark operated in the hybrid mode. These results show the formation of a Z-pinch column extending from the cathode to midpoint of the discharge. There is good agreement as far as dimensions and time are concerned with the streak camera results presented here. The laser probe pulse in the interferometric measurements was rather long, and it was not possible to resolve either small-scale or rapid plasma formations in our previous experiment.[5] The mean electron density in the 200 μm diam pinch was found to be approximately 1×10^{19} cm^{-3}. Optical shadowgrams have shown smaller-scale point-like structures within the same Z-pinch column. The limited optical resolution, however, has not allowed resolution better than 50 μm in these experiments. The same series of interferograms show that before the formation of this column there is a larger diameter plasma whose electron density is at least an order of magnitude lower. The series of interferograms of Ref. 5 were taken on different shots, and so it was not strictly possible to affirm a Z-pinch compression, although the results are consistent with the optical evidence, presented in this work, of a collapsing Z-pinch shell in the time leading up to peak current. Interferograms presented in Ref. 5 also show the development of an off-axis optically dense plasma propagating from the anode, close to the time of peak current, as well as a plasma with a diameter of several millimeters within a millimeter of the cathode surface. It may be concluded that within the limits of comparability, the two diagnostics do show considerable agreement.

The different radial velocities of the implosion velocity of the Z pinch requires comment. This effect may be explained if a nonuniform axial density is postulated. A significantly lower ion density in the central part of the discharge would explain the faster pinch compression observed from the $\mathbf{J}\times\mathbf{B}$ force. As the material to be compressed in the pinch must come from either one, if not both, of the electrodes before the pinching starts, the mean axial ion velocity will be important in determining the time to reach the density conditions required for micropinch formation. The thermal ion velocity of titanium at 100 eV, which is an order of magnitude representative value, for example, is only 2×10^6 cm s^{-1}, which means that a time of the order of 250 ns is required to reach a uniform axial density. This time is quite long on the current growth time scale of the present experiment, and a nonuniform axial density may be inferred. It may then be expected that the ion density will be lower at the midpoint of the discharge. If this is the case, a simple snowplow model will explain the maximum values of the compressional velocity found here. The source of ions from the anode is, initially at least, from electron beam–target interaction. This is especially important in the first part of the current ramp. In the experimental observations presented here, this corresponds to the energetic x-ray emission of about 5 ns duration seen immediately following the laser preionizing pulse; at which time the applied gap voltage is approximately 80 kV. The laser incident on the cathode is sufficient to liberate the order of 3×10^{17} ions. This value is sufficient to permit an initial density of order 1×10^{18} cm^{-3} just prior to the compression phase in the Z-pinch channel. This value of the initial density is consistent with the results of Ref. 5.

The radial velocity has been observed using a streak camera in a conventional low inductance vacuum spark.[10] There are, however, considerable differences with the results presented here for the plasma dynamics. In this earlier work, the laser was focused onto the anode. The radial streaks show that the radial pinching at different axial locations differs in its temporal behavior. At the time when the plasma close to the anode becomes fully pinched, the plasma 2 mm farther toward the cathode, which is at a position near the midpoint of the discharge, is only beginning to implode. Axial streaks shown in the same publication indicate that a bright luminous front, believed to consist of plasma of the anode material, moves toward the cathode with a velocity of between 0.5 and 1.0×10^{6} cm s^{-1}. It is suggested that the plasma points are formed at the boundary of the moving anode plasma. While the observations from the axial streaks presented in this work do show that plasma from the anode propagates toward the cathode, the micropinches are to be seen in a plasma that is propagating from the cathode toward the anode. The location of maximum compression, as presented in Ref. 10, propagates toward the anode, with a velocity of about 4×10^{6} cm s^{-1}. The compression is seen to occur approximately 900 ns from the start of the current pulse, with maximum compression and x-ray emission approximately 100 ns later.

Apart from the difference in time scale for the two experiments, the most significant difference is where the laser is focused. It may be noted that, when the laser is focused onto the anode in the hybrid mode, no x-ray emission from the interelectrode volume is recorded. Intense and comparatively hard x-ray emission is observed from the anode surface due to beam–target electron interaction. The discharge impedance is noticeably higher for these conditions. In addition, the plasma densities substantially lower than the case of laser illumination of the cathode, and are too low to be detected by green light interferometry. The same behavior is also seen in the case when the line is operated in the switched mode, that is, with the line gap present. In this latter case, the current pulse lengths are even shorter. Observations on fast pulse power-driven discharges find the micropinches either near the midpoint[3] or closer to the cathode.[4] The situation in capacitor-driven low inductance vacuum spark discharges is usually, but by no means always, that the micropinch formation is observed near the anode. This is the case of experiment of Ref. 11. The different time scales of the current waveform in the two classes of generator are clearly significant. In the case of the capacitor bank driven low inductance discharges, the density may easily reach a nearly uniform value in the whole gap volume before the current reaches the 100 kA level, where plasma hot spots and micropinches are observed. Thus, a laser pulse incident on the anode is an effective means of operating the vacuum spark for a capacitor bank driven machine. In the case of both hybrid and normal operation of a pulse power driven discharge, the time scales are an order of magnitude shorter, and the mean axial ion velocity can become a determining factor.

The observation of an off-axis plasma, which is observed to intensify on the pinching of the Z-pinch column, may be explained by recalling that the discharge cross section is reduced markedly at this time. There will be corresponding increase in the impedance of the discharge, and the current will seek alternative paths. Any asymmetry or field enhancement will be the location of an alternative current path. The edge of the anode cone is a suitable site for an enhanced electric field.

The best information about the dimensions of a micropinch has been obtained by x-ray pinhole measurements. The micropinch size distribution for a titanium plasma has been found to depend on current.[11] For a maximum current of 100 kA, the most probable size is between 10 and 20 μm, with a distribution of rather more diffuse hot spots with a diameter of 100–200 μm. These measurements were made on a conventional capacitor bank discharge, but the behavior is reproduced in the present work. If the authors' argument is followed, and the initial line density is approximately conserved during the collapse phase of radiative collapse, then it may be inferred that the density will reach 1×10^{21} cm^{-3}.

The very close correspondence between the x-ray and the light signal from the Z-pinch column requires some explanation. Given the high temperature of the micropinch plasma, all visible light output will be from free–free bremsstrahlung. The recombination component is insignificant.[12] The emission is, then, proportional to $n_e\cdot n_i\cdot T^{-0.5}$. The temperature variation is expected to be comparatively slow compared to the radiative collapse time scale, which is approximately the rise time of the x-ray PIN diode signal. Simulations have shown[13] that, during the nanosecond time scale of the micropinch, the temperature may increase by up to an order of magnitude, while the density will change by three to four orders of magnitude. It may be concluded that, for electron densities well below the critical density of 4×10^{21} cm^{-3} for green light, the light signal provides an approximate measure of the product of the densities of both species. The most probable degree of ionization as predicted by RATION,[9] for the densities expected, varies from about 14+ at 200 eV to 19+ at 700 eV, which is the characteristic temperature obtained from the x-ray pinhole camera images. The pinch plasma in which the micropinches form has been measured by interferometry[4] to have a density of 1×10^{19} cm^{-3}. The light intensity increase, in the two nanosecond time scale of the formation of the micropinch, is approximately a factor of 300. If the temperature is taken as approximately constant, a lower bound on the density may be put at 2×10^{20} cm^{-3}. If the temperature is taken to increase by an order of magnitude during the radiative collapse phase, as is indicated by the theoretical model, then a lower bound on the density is increased by a factor of 3. Such a value of the density is in agreement with the densities obtained in spectroscopic measurements of the x-ray emission shape and ratios.[14] It is also in agreement with the argument that the line density is approximately constant on the nanosecond, 1–3 ns, time scale of a micropinch event.

V. CONCLUSIONS

The observations of the vacuum spark made with an optical streak camera have shown a rich variety of behavior in term of the axial position. Each of these zones may be recognized by the behavior of the plasma velocities, both radial and axial. The comparison of the soft x-ray emission with the optical emission identify the characteristic micropinch x-ray emission with a band of bright optical spots propagating from close to the cathode toward the anode. The greater part of the x-ray emission comes from this region at this time. Each micropinch observed on a pinhole camera image of a single shot corresponds to a unique event at that point. The streak camera observations may be compared with previous observations of the electron density using Holographic Interferometry. The streak camera observations do allow the dynamics of the formation of the Z-pinch column, in which the micropinches form, to be observed.

The temperature and densities of the micropinch may be estimated with reasonable precision. It was not possible, however, to establish the minimum diameter of the micropinch with the same degree of precision.

The behavior of the vacuum spark driven by a pulse forming line and operating in the hybrid mode is found to exhibit a different behavior to the vacuum spark driven by a low inductance capacitor bank. The different dynamic behavior is particularly obvious on considering the difference in the radial collapse velocity as a function of axial position.

ACKNOWLEDGMENTS

The authors thank Dr. Peter Choi for many stimulating discussions.

The authors wish to thank the Chilean Research Agency, FONDECYT, for their funding under Grant No. 1930557, and the European Economic Community under their grant, No. C11*-CT92-0053.

[1] E. D. Korop, B. E. Meierovich, Yu. V. Sidel'nikov, and S. T. Sukorukov, Sov. Phys. Usp. **22**, 727 (1979).
[2] K. N. Koshelev and N. R. Pereira, J. Appl. Phys. **69**, R21 (1991).
[3] S. M. Zakharov, G. V. Ivanenkov, A. A. Kolomenskii, S. A. Pikuz, and A. I. Samokhin, Sov. J. Plasma Phys. **10**, 303 (1984).
[4] H. Chuaqui, M. Favre, L. Soto, and E. Wyndham, Phys. Fluids B **5**, 4244 (1993).
[5] E. Wyndham, H. Chuaqui, M. Favre, L. Soto, and P. Choi, J. Appl. Phys. **71**, 4164 (1992).
[6] M. Favre, S. Lee, S. P. Moo, and C. S. Wong, Plasma Sources Sci. Technol. **1**, 122 (1992).
[7] V. A. Veretenikov, S. N. Polukhin, O. G. Semenov, and Yu. V. Sidel'nikov, Sov. J. Plasma Phys. **7**, 656 (1981).
[8] P. Choi and C. Dumitrescu Zoita (private communication) to be submitted to Rev. Sci. Instrum.
[9] R. W. Lee, B. L. Whitten, and R. E. Strout, J. Quant. Spectrosc. Radiat. Transfer **32**, 91 (1984).
[10] T. N. Lee, Ann. NY Acad. Sci. **251**, 112 (1975).
[11] P. S. Antsiferov, K. N. Koshelev, A. E. Kramida, and A. M. Panin, J. Phys. D Appl. Phys. **22**, 1073 (1989).
[12] P. J. Brussard and H. C. van de Hulst, Rev. Mod. Phys. **34**, 507 (1962).
[13] V. V. Vikhrev, V. V. Ivanov, and K. N. Koshelev, Soc. J. Plasma Phys. **8**, 688 (1982).
[14] V. A. Veretennikov, V. A. Gribkov, E. Ya. Kononov, O. G. Semenov, and Yu. V. Sidel'nikov, Sov. J. Plasma Phys. **7**, 249 (1981).